On the Ce–Mn clustering in CaF_2 in which the $Ce^{3+} \rightarrow Mn^{2+}$ energy transfer occurs

2003 J. Phys.: Condens. Matter 15 3821

(http://iopscience.iop.org/0953-8984/15/22/316)

INSTITUTE OF PHYSICS PUBLISHING JOURNAL OF PHYSICS: CONDENSED MATTER

J. Phys.: Condens. Matter **15** (2003) 3821–3830 PII: S0953-8984(03)57814-6

On the Ce–Mn clustering in CaF_2 in which the $Ce^{3+} \rightarrow Mn^{2+}$ energy transfer occurs

U Caldiño G

Departamento de Física, Universidad Autónoma Metropolitana-Iztapalapa, PO Box 55-534, 09340 México, DF, Mexico

E-mail: cald@xanum.uam.mx

Received 3 January 2003, in final form 31 March 2003
Published 23 May 2003
Online at stacks.iop.org/JPhysCM/15/3821

Abstract

Energy transfer from Ce^{3+} to Mn^{2+} ions in a single crystal of CaF_2 co-doped with cerium and manganese ions has been analysed. The spectroscopic data obtained clearly indicate that sensitized luminescence with cerium ions as sensitizers and manganese ions as activators takes place between Ce^{3+}–Mn^{2+} clusters formed in the crystalline matrix. The number of such clusters was estimated using a simple model in which both ions are treated as two-energy-level systems. Some insight into the possible nature of the Ce^{3+}–Mn^{2+} complexes as well as of the $Ce^{3+} \rightarrow Mn^{2+}$ energy transfer mechanism taking place inside them were gathered using Dexter's theory for energy transfer phenomena.

1. Introduction

The study of resonant energy transfer among impurity ions in a solid material has been an area of intense research during recent decades, mainly because of its importance in the development of efficient phosphor materials (for alphanumeric displays, visual display screens and radiation detectors), optical frequency converters and solid state lasers.

Because of its versatile spectroscopic properties, the Ce^{3+} ion has been used as a sensitizer in energy transfer processes taking place in diverse halide crystals. For example, an efficient sensitization of the luminescence of Eu^{2+} ions by Ce^{3+} ions in monocrystalline CaF_2 was found even for a very low concentration (<1 ppm) of Eu^{2+} ions [1]. Moreover, calcium fluoride is a compound with a simple structure, which has high solubility of both sensitizer and activator ions permitting preparation of efficient phosphor samples over a wide range of concentrations. It therefore appears to be ideally suited to the investigation of sensitized luminescence. Rare-earth ions trivalent (Re^{3+}) enter the CaF_2 lattice substitutionally for Ca^{2+} and may reside in a variety of sites. Non-locally compensated Re^{3+} ions form centres of cubic symmetry (O_h).

The ion may also be charge compensated by F^- interstitials in either nearest-neighbour or next-nearest-neighbour positions, forming tetragonal (C_{4v}) or trigonal (C_{3v}) centres respectively. As a consequence, clustering of such defects readily occurs, resulting in a variety of possible cluster configurations.

The optical properties of Ce^{3+} in CaF_2 have been previously analysed by several workers. The absorption spectrum at low concentrations of Ce^{3+} ions mainly consists of two bands labelled A (peaking at ∼305 nm) and B (peaking at ∼200 nm) in increasing order of energy. Loh [2] attributed such bands to the $4f \rightarrow 5d$ absorption of Ce^{3+} ions charge compensated by F^- interstitials in nearest-neighbour positions forming tetragonal centres (Ce^{3+}–F^-_{int} centres). As the cerium concentration increases, two additional bands called C (peaking at ∼240 nm) and D (peaking at ∼218 nm) appear in the absorption spectrum. These two bands have been associated with the $4f \rightarrow 5d$ transitions of Ce^{3+}–F^-_{int} ions forming aggregates of an unknown structure in the crystalline matrix. Excitation within either the A or B absorption bands induces the emission characteristic of the Ce^{3+} ions in tetragonal sites, which consists of two bands peaking at 320 and 340 nm. These bands are associated with transitions from the $^2D_{3/2}$ excited level to the ^2F ground state, which is split into its $^2F_{5/2}$ and $^2F_{7/2}$ components by spin–orbit interaction [1].

On the other hand, although the Mn^{2+} $d \rightarrow d$ absorption transitions are difficult to pump, since they are forbidden by spin and parity for electric dipole radiation in octahedral complexes, such ions have played an important role as activators of important phosphor materials, such as the CaF_2:Mn^{2+}, widely used as a thermoluminescent dosimeter. Mn^{2+} enters substitutionally for Ca^{2+}, which has an eightfold coordination environment. The absorption (excitation) bands observed in the excitation spectrum of the Mn^{2+} emission in CaF_2 have been attributed to transitions from the Mn^{2+} ground state $^6A_{1g}(S)$ to different excited levels in a cubic environment [3, 4]. Previously, it has been found that efficient pumping of Mn^{2+} ions in CaF_2 can be achieved using Eu^{2+} [5] or Ce^{3+} [6, 7] ions as sensitizers. McKeever *et al* [6, 7] presented for the first time in the CaF_2:Ce^{3+}:Mn^{2+} phosphor material clear evidence that $Ce^{3+} \rightarrow Mn^{2+}$ energy transfer takes place predominantly from Ce^{3+} ions charge compensated by F^- interstitials in nearest-neighbour positions forming tetragonal centres (C_{4v}). In fact, in CaF_2 such C_{4v} centres appear to be dominant for all rare earths [8].

In the present investigation, a spectroscopic study of the Ce^{3+}-sensitized Mn^{2+} luminescence in monocrystalline CaF_2 is presented. The possible nature of the Ce^{3+}–Mn^{2+} clusters in which the energy transfer takes place, as well as the possible mechanisms for such a process, are discussed. The study of such a system is important to find more effective phosphor materials which could be used in efficient UV–visible optical conversion devices.

2. Experimental details

The single crystals of CaF_2:Ce^{3+} and CaF_2:Ce^{3+}:Mn^{2+} employed in this investigation were grown by Optovac Inc. using a double-crucible technique to minimize oxygen contamination. Standard mechanical polishing techniques utilizing alumina polishing abrasives were used to prepare crystal surfaces for optical measurements. The cerium concentration was determined from their A absorption band using Smakula's equation with a value for the oscillator strength of 4.8×10^{-3} [7]. The result was $\sim 2.4 \times 10^{18}$ cm^{-3}, which corresponds to about 90% of the Ce^{3+} added to the melt, and therefore the remaining Ce^{3+} ions can be accounted for by Ce^{3+} aggregates associated with the C and D bands. Such an estimation was achieved using a Perkin Elmer λ-5 double-beam recording spectrophotometer. The manganese ion concentration was determined by atomic absorption spectrophotometry.

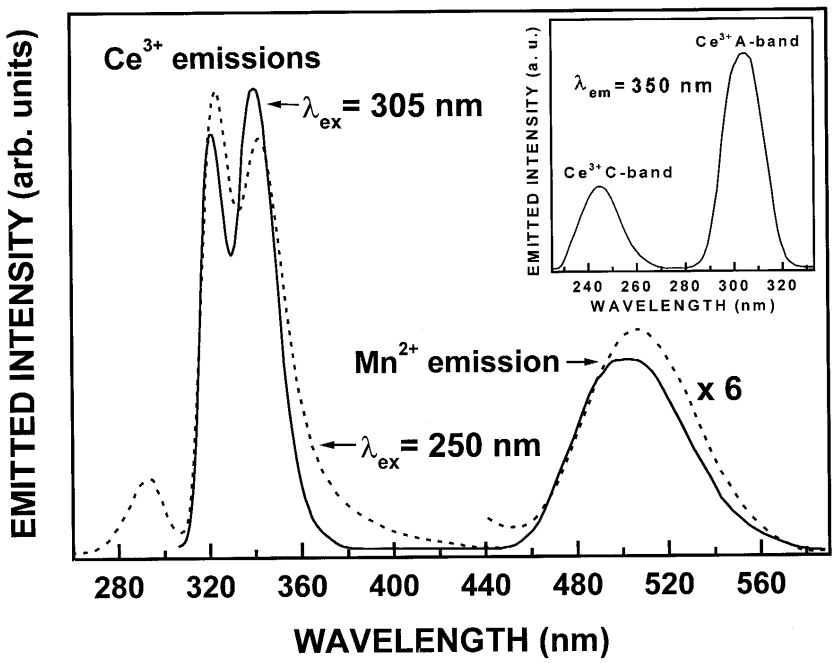

Figure 1. RT emission spectra under excitation within the Ce^{3+} A band at 305 nm (——) and within the C band at 250 nm (- - - -). The inset shows the excitation spectrum of the Ce^{3+} emission taken at 350 nm.

Continuous emission and excitation spectra were obtained with a Perkin-Elmer 650-10S spectrofluorimeter equipped with a 150 W xenon lamp and a red-sensitive Hamamatsu R928 photomultiplier tube. Such spectra were corrected for the energy response of the excitation source using an anthracene crystal, and for the energy response of the emission detector using a calibrated light source. Lifetime data for the cerium and manganese emissions were gathered using a 250 W pulsed xenon lamp (Oriel model 66057). The resulting transient fluorescence signal was analysed with a 0.45 m Czerny–Turner monochromator, detected with a cooled Hamamatsu R943-03 photomultiplier tube and processed by a Hewlett Packard model 54201A digitizing oscilloscope. Low-temperature measurements were made with an Air Products DE-202 He closed-cycle cryostat refrigerator.

3. Results

Figure 1 portrays the room-temperature (RT) emission spectra of a CaF_2:Ce^{3+} ($\sim$170 ppm):Mn^{2+} ($\sim$3500 ppm) crystal excited at 305 and 250 nm. By exciting the crystal within the A absorption band, at 305 nm, two ultraviolet (UV) bands, peaking at $\sim$320 and 342 nm, and a green band, peaking at $\sim$502 nm, were observed. The UV bands correspond to the de-excitation of Ce^{3+}–F^-_{int} ions from the excited state $^2D_{3/2}$ to the split ground state into their $^2F_{5/2}$ and $^2F_{7/2}$ components. The green band was found to shift to longer wavelengths when the sample temperature was lowered. This behaviour is usually observed for the Mn^{2+} emission. The green band was, therefore, attributed to the $^4T_{1g}(G) \rightarrow {}^6A_{1g}(S)$ transition of Mn^{2+} ions. Excitation at 250 nm, within the C-absorption band, produces two additional UV bands peaking at about 293 and 380 nm.

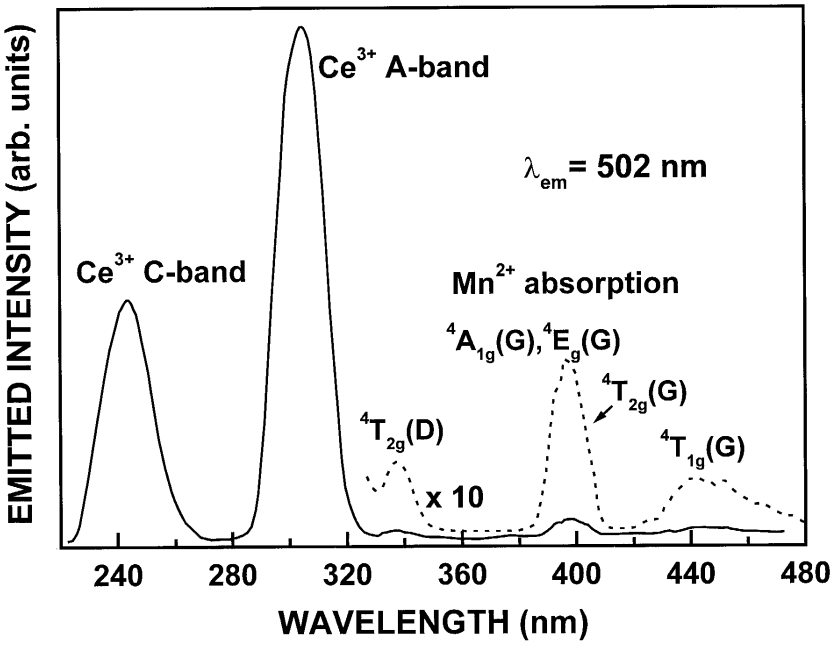

Figure 2. RT excitation spectrum of the Mn^{2+} emission taken at 502 nm.

The RT excitation spectrum corresponding to the 320 and 342 nm UV emission bands presents two bands peaking at ∼245 and 303 nm. Such an excitation spectrum monitored at $\lambda_{em} = 350$ nm is displayed in the inset of figure 1. The higher energy band corresponds to the C absorption band of tetragonal Ce^{3+} ions forming aggregates. The 303 nm band corresponds to the A absorption band of tetragonal Ce^{3+} ions. Figure 2 displays the RT excitation spectrum of the green emission band, taken at $\lambda_{em} = 502$ nm, which not only contains the $^6A_{1g}(S) \rightarrow {}^4T_{1g}(G)$, $^6A_{1g}(S) \rightarrow {}^4T_{2g}(G)$, $^6A_{1g}(S) \rightarrow {}^4A_{1g}$, $^4E_g(G)$ and $^6A_{1g}(S) \rightarrow {}^4T_{2g}(D)$ absorption transitions of Mn^{2+} ions, but also the A absorption band of tetragonal Ce^{3+} ions. The C absorption band is also present in this spectrum, and therefore the Ce^{3+}–F^-_{int} ion aggregates also take part in energy transfer to Mn^{2+} ions.

The Ce^{3+} ion luminescence peaking at 320 and 342 nm consisted of a single decay constant with a lifetime which was determined to be about 1 μs at RT. On the other hand, such a Ce^{3+} luminescence in a sample having no manganese present also exhibited a pure exponential decay with a lifetime which was determined to be equal, within experimental error (±5%), to that measured for the Ce^{3+} emission in the doubly doped crystal.

The manganese luminescence decay was found to consist of a single exponential decay with no observable rise time. The time constant of the decay which corresponds to the lifetime of the $^4T_{1g}(G)$ excitation level of Mn^{2+} increased from 84 ± 8 ms at RT to 159 ± 15 ms at 20 K. This decay scheme was found to be similar to that determined in a powder sample of CaF_2:Mn^{2+} (∼5000 ppm) [5]. It is also similar to that reported by Alonso and Alcalá [9] in single crystals of CaF_2:Mn^{2+} (∼5000 ppm). The decrease in the lifetime of the Mn^{2+} emission when the sample temperature is increased from 20 K to RT can be explained considering that the probabilities of the phonon-assisted and non-radiative processes are enhanced with increasing in temperature.

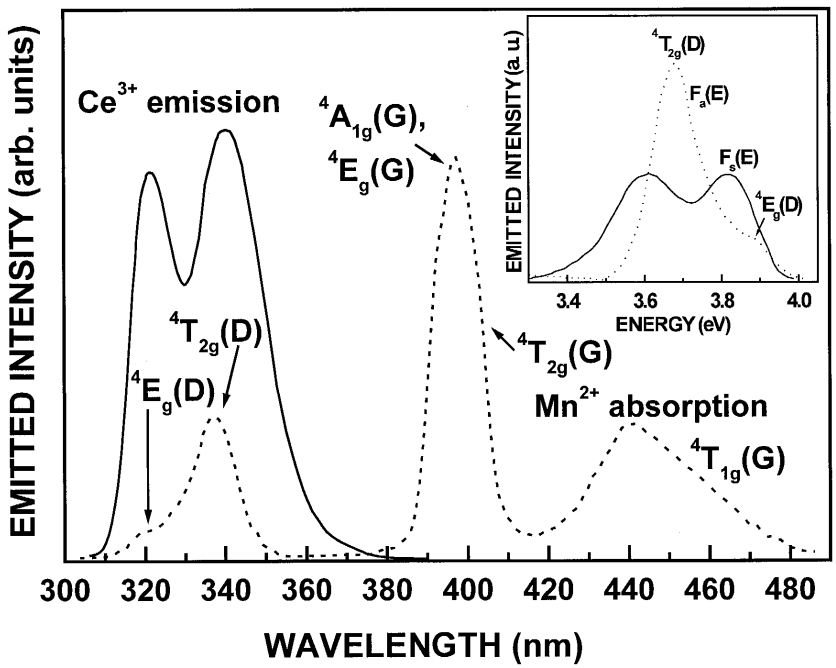

Figure 3. RT overlap region between cerium emission (——) and manganese absorption (- - - -). The inset shows the normalized shape functions.

4. Discussion

The more significant experimental data can be summarized as follows:

(a) Taking into account that the Mn^{2+} emission is produced under A-band excitation of Ce^{3+}–F^-_{int} ions (at 305 nm), in which the Mn^{2+} ions cannot be excited, then an efficient sensitization of the luminescence of Mn^{2+} ions by tetragonal Ce^{3+} ions is achieved in the lattice of CaF_2. Such a process is expected to occur since the Ce^{3+} emission produced by A-band excitation overlaps the $^6A_{1g}(S) \rightarrow {}^4T_{2g}(D)$ and $^6A_{1g}(S) \rightarrow {}^4E_g(D)$ Mn^{2+} absorptions, as can be appreciated from the spectrum shown in figure 3. However, for low concentrations of impurity ions, the interaction distance between sensitizer Ce^{3+} and activator Mn^{2+} ions calculated from a truly random distribution of the impurities is large ($\sim$25 Å), such that the $Ce^{3+} \rightarrow Mn^{2+}$ energy transfer should not have occurred. Thus, the observation of such a transfer suggests that the impurities are not randomly distributed in the lattice, but rather occur as Ce^{3+}–Mn^{2+} impurity clusters.

(b) The manganese emission in the CaF_2:Ce^{3+}:Mn^{2+} crystal induced by $Mn^{2+6}A_{1g}(S) \rightarrow {}^4T_{2g}$ (D) absorption, at 340 nm, peaks at a shorter wavelength (at $\sim$490 nm) than the Ce^{3+}-sensitized Mn^{2+} emission (at $\sim$502 nm). This result was also observed by McKeever *et al* [7], who suggested that the Ce^{3+} ion (1.07 Å) larger than the Ca^{2+} ion (0.98 Å) should involve an increased ligand field around the Mn^{2+} ions (0.8 Å), which in turn should produce a larger crystal field splitting of the manganese ^4G energy levels, and hence a longer wavelength emission. This explanation seems to be reasonable if the Mn^{2+} and tetragonal Ce^{3+} ions predominantly cluster at first or second neighbours.

(c) The decay pattern of the Ce^{3+} luminescence in CaF_2:Ce^{3+} is not affected by the presence of Mn^{2+} ions in the doubly doped crystal.

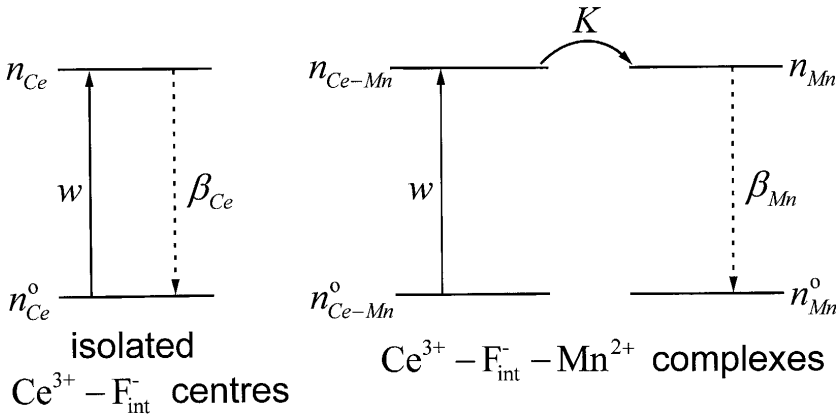

Figure 4. Energy level system used to describe the kinetics of $Ce^{3+} \rightarrow Mn^{2+}$ energy transfer.

(d) The total integrated emission of the Ce^{3+} ions is reduced by the presence of the Mn^{2+} ions.
(e) Pulse excitation of Ce^{3+} resulted in a Mn^{2+} luminescence with no observable rise time. Considering the sensitivity and the overall time of our experimental set-up, this result indicated that the rise time of the Mn^{2+} fluorescence was less than 25 ns.

On the basis of these observations a model describing the essential features of the kinetics of $Ce^{3+} \rightarrow Mn^{2+}$ energy transfer can be built. In this model, which is depicted in figure 4, both the sensitizer cerium and activator manganese ions are treated as two energy-level systems. In order to incorporate observations (c) and (d) the model considers that for coupled Ce^{3+}–Mn^{2+} ions the energy transfer from the cerium to the manganese ions proceeds at a rapid rate that quenches the sensitizer emission. On the other hand, the isolated cerium ions are, on average, at a distance from the manganese ions such that no energy transfer can take place, hence leaving the lifetime of the cerium ions unchanged. This situation means that cerium ions clustered with manganese ions do not exhibit any fluorescence. Thus, the observed cerium emission originates exclusively from these ions, which are not interacting with Mn^{2+} ions, and the observed green emission is due to the to the $^4T_{1g}(G) \rightarrow {}^6A_{1g}(S)$ transition of Mn^{2+} ions, which results from excitation by energy transfer from tetragonal cerium ions forming the impurity clustering.

According to this model, the rate equations describing the time evolution of the excited-state populations of both isolated cerium ions and Ce–Mn complexes are given by

$$\begin{aligned} \frac{dn_{Ce}}{dt} &= wn^o_{Ce} - \beta_{Ce} n_{Ce}, \\ \frac{dn_{Ce-Mn}}{dt} &= wn^o_{Ce-Mn} - Kn_{Ce-Mn}, \\ \frac{dn_{Mn}}{dt} &= Kn_{Ce-Mn} - \beta_{Mn} n_{Mn}, \end{aligned} \tag{1}$$

where n_{Ce} and n_{Ce-Mn} are the concentrations of excited state Ce^{3+} ions in isolated and coupled form respectively, n^o_{Ce} and n^o_{Ce-Mn} are the corresponding populations for the ground state, n_{Mn} is the concentration of excited state Mn^{2+} ions forming Ce–Mn complexes, w is the absorption probability, which is assumed to be the same for both isolated and coupled Ce^{3+} ions, K is the rate of energy transfer, and β_{Ce} and β_{Mn} are the fluorescence decay rates of the isolated cerium and coupled manganese ions. Mn^{2+} emission was produced under A-band excitation of Ce^{3+}–F^-_{int} ions avoiding direct excitation of Mn^{2+} ions.

Equations (1) can be easily solved for continuous excitation to give the steady-state populations: $n_{Ce} = wn^o_{Ce}/\beta_{Ce}$ and $n_{Mn} = wn^o_{Ce-Mn}/\beta_{Mn}$. Considering that the fluorescence intensity of a specific level is equal to the product of the population and the radiative decay rate (β^r) of the level, the ratio for the emission intensities of the Mn^{2+} ions (I_{Mn}) and the isolated Ce^{3+} ions (I_{Ce}) in the limit of weak pumping, where $n^o_{Ce} \approx N_{Ce}$ and $n^o_{Ce-Mn} \approx N_{Ce-Mn}$, is given by:

$$\frac{I_{Mn}}{I_{Ce}} = \frac{(\beta^r_{Mn}/\beta_{Mn})N_{Ce-Mn}}{(\beta^r_{Ce}/\beta_{Ce})N_{Ce}}, \tag{2}$$

where N_{Ce} and N_{Ce-Mn} are the total concentrations of isolated and coupled Ce^{3+} ions respectively.

The ratio for the number of Ce^{3+} ions which should be associated with Mn^{2+} ions (N_{Ce-Mn}) and the total concentration of cerium ($N_T = N_{Ce} + N_{Ce-Mn}$) in the crystal can be obtained from equation (2) after some minor manipulations:

$$\frac{N_{Ce-Mn}}{N_T} = \frac{(I_{Mn}/I_{Ce})(\beta^r_{Ce}/\beta_{Ce})}{\beta^r_{Mn}/\beta_{Mn} + (I_{Mn}/I_{Ce})(\beta^r_{Ce}/\beta_{Ce})}. \tag{3}$$

Using $\beta_{Mn} \approx 2\beta^r_{Mn}$ and $\beta^r_{Ce} \approx \beta_{Ce}$ [10], N_{Ce-Mn}/N_T resulted to be about 0.11 when our experimentally determined ratio for $I_{Mn}/I_{Ce} = 0.06$ was used in equation (3). Therefore, about 11% of the total concentration of Ce^{3+} ions appears to be associated with Mn^{2+} ions.

Let us now discuss the possible mechanism for the $Ce^{3+} \rightarrow Mn^{2+}$ energy transfer. Considering that the Ce–Mn complex transfer rate K is time-independent, solutions to the rate equations (1) can be obtained under the assumption that ω represents a delta function excitation pulse:

$$n_{Ce-Mn}(t) = n^o_{Ce-Mn}\exp(-Kt), \tag{4}$$

$$n_{Mn}(t) = \frac{Kn^o_{Ce-Mn}}{\beta_{Mn} - K}[\exp(-Kt) - \exp(-\beta_{Mn}t)]. \tag{5}$$

The time at which the activator fluorescence intensity reaches its maximum value (t_{max}) can be determined by setting the first time derivative of $n_{Mn}(t)$ equal to zero, resulting in:

$$t_{max} = \frac{1}{K - \beta_{Mn}}\ln\left(\frac{K}{\beta_{Mn}}\right). \tag{6}$$

From this equation and our experimentally determined data, $t_{max} < 25$ ns and $\beta_{Mn} = 11.9\ s^{-1}$, the rate of $Ce^{3+} \rightarrow Mn^{2+}$ energy transfer was estimated to be greater than $7.1 \times 10^8\ s^{-1}$. On the other hand, Dexter [11] demonstrated that dipole–dipole interactions can generally be expected to dominate the energy transfer mechanism when both the sensitizer and activator ions have dipole-allowed transitions. However, the long lifetime measured for the manganese emission reveals the forbidden nature of the 3d → 3d transitions. Therefore, it might be expected that the $Ce^{3+} \rightarrow Mn^{2+}$ energy transfer mechanism is of the electric dipole–quadrupole type. The transfer rate W^{DQ}_{sa} for the electric dipole–quadrupole interaction is related to the transfer rate W^{DD}_{sa} for the electric dipole–dipole interaction through the following relation [11]:

$$W^{DQ}_{sa} = \left(\frac{\lambda_s}{R_{sa}}\right)^2\left(\frac{f_q}{f_d}\right)W^{DD}_{sa}, \tag{7}$$

where λ_s is the wavelength position of the sensitizer emission, R_{sa} is the distance between the ions involved in the transfer, and f_q and f_d are the oscillator strengths of the activator

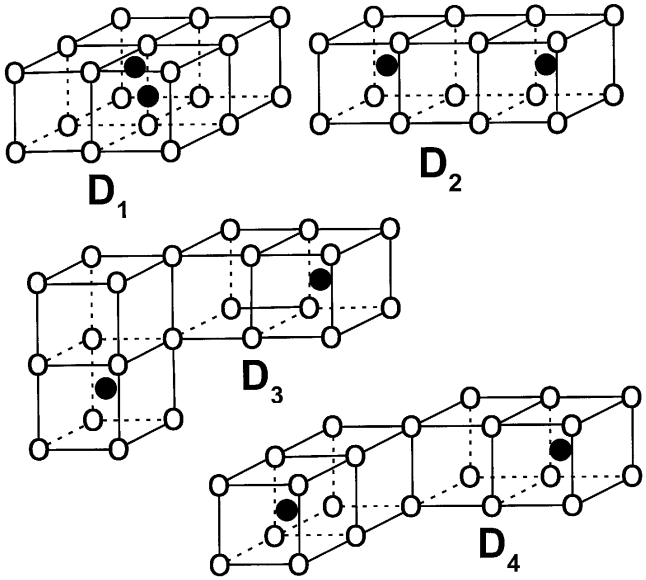

Figure 5. Four of the simplest configurations for the Ce–Mn complex in the CaF_2 lattice, which were considered to calculate the rate of energy transfer via electric multipolar interaction mechanisms.

quadrupole and dipole electrical transitions respectively. The expression for the electric dipole–dipole transfer probability W_{sa}^{DD} is given by [11]:

$$W_{sa}^{DD} = \frac{3\hbar^4 c^4}{4\pi n^4 \tau_s^o}\left(\frac{1}{R_{sa}}\right)^6 Q_a \Omega(F_s, F_a), \tag{8}$$

where we have assumed that the field strength in the medium is equal to that in air. τ_s^o is the sensitizer intrinsic lifetime in the absence of energy transfer, Q_a is the integrated absorption coefficient of the manganese ions, and $\Omega(F_s, F_a) = \int [F_s(E)F_a(E)/E^4]\,\mathrm{d}E$ represents the spectral overlap between the normalized shapes of the Ce^{3+} emission $F_s(E)$ and Mn^{2+} absorption $F_a(E)$. The other symbols in equation (8) have their usual meaning. Because the small absorption coefficient of manganese is difficult to measure, Q_a was estimated using the relationship $Q_a = 4.8 \times 10^{-16} f_d$ derived by Blasse [12], where $f_d \sim 10^{-7}$ for Mn^{2+} ions. The overlap integral was calculated using the RT cerium emission and manganese absorption spectra portrayed in figure 3. The normalized line-shape functions for the Ce^{3+} emission and Mn^{2+} absorption in the overlap region are displayed in the inset of the same figure. To obtain $F_a(E)$ we employed the excitation spectrum of Mn^{2+} in CaF_2 reported by Alonso and Alcalá [9]. The value of Ω was found to be 1.2×10^{-2} eV^{-5}.

Now, taking into account that $f_d \sim 10^{-7}$ and $f_d \sim 10^{-10}$ for Mn^{2+} ions, and using the fluorescence decay datum for the cerium emission and the values for Q_a and Ω mentioned above, the critical interaction distance (defined as the distance at which the energy transfer rate is equal to the intrinsic rate of the sensitizer ions, i.e. $W_{sa}^{DQ}\tau_s^o = 1$) was estimated from equations (7) and (8). This interaction distance, which resulted to be ∼9.2 Å, is smaller than that obtained (∼25 Å) assuming a random distribution of Ce^{3+} and Mn^{2+} ions. It can be inferred, therefore, that the $Ce^{3+} \rightarrow Mn^{2+}$ energy transfer arises from small Ce–Mn clusters instead of from randomly distributed ions.

Table 1. Calculated rates of $Ce^{3+} \rightarrow Mn^{2+}$ energy transfer in CaF_2 at 300 K using electric multipolar interaction mechanisms and the complex configurations shown in figure 5.

Complex	Interaction distance (Å)	Energy transfer rate (s^{-1})	
		W_{sa}^{DD}	W_{sa}^{DQ}
D_1	3.86	1.4×10^6	1.0×10^9
D_2	5.45	1.8×10^5	6.6×10^7
D_3	6.68	5.2×10^4	1.3×10^7
D_4	7.71	2.2×10^4	4.1×10^6

Since the exact nature of the Ce–Mn clusters cannot be inferred from our optical data, different kinds of small clusters in which the Ce^{3+} and Mn^{2+} ions are separated by at most 9 Å can be imagined in the CaF_2 lattice. Some of the simplest configurations are illustrated in figure 5. The rate of $Ce^{3+} \rightarrow Mn^{2+}$ energy transfer via an electric dipole–quadrupole interaction mechanism was calculated using these dimer configurations. The results obtained are given in table 1, where the energy transfer rates calculated using an electric dipole–dipole interaction mechanism are also included for comparison. As expected, more reasonable values are obtained when a dipole–quadrupole interaction mechanism is employed rather than an electric dipole–dipole one. Moreover, the closer agreement between the calculated and experimental values for W_{sa}^{DQ} is achieved when it is assumed that the Mn^{2+} ion occupies the positions of first neighbours to the cerium ion, as is the case in the complex D_1 in figure 5.

Finally, it is important to note that the calculated rates of $Ce^{3+} \rightarrow Mn^{2+}$ energy transfer via a dipole–quadrupole interaction mechanism in the complexes D_1 and D_2, portrayed in figure 5, were found to be quite high as compared with the intrinsic radiative decay rate of the Ce^{3+} ions ($\sim 1 \times 10^6$ s^{-1}). This result supports the assumption mentioned above that the cerium emission is quenched by energy transfer to manganese ions forming impurity clusters.

5. Conclusions

The spectroscopic data obtained for CaF_2:Ce^{3+} ($\sim$170 ppm):Mn^{2+} ($\sim$3500 ppm) indicate that the $Ce^{3+} \rightarrow Mn^{2+}$ energy transfer process taking place in this material occurs due to some tendency for the Ce^{3+} and Mn^{2+} ions to form small Ce–Mn complexes. In fact, our experimental data can only be explained assuming that a short-range interaction mechanism such as an electric dipole–quadrupole interaction occurs in the Ce–Mn clusters. This impurity clustering, which has been considered to be infrequent in most studies of energy transfer between impurities in solids, appears to be quite a relevant finding for the design of more efficient phosphor and laser systems.

Acknowledgments

The author thanks professor S W S McKeever from Oklahoma State University, who kindly supplied the single crystals of CaF2:Ce and CaF_2:Ce, Mn, and I Camarillo for his technical assistance.

References

[1] Caldiño U G, de la Cruz C, Muñoz G H and Rubio J O 1989 *Solid State Commun.* **69** 347
[2] Loh E 1966 *Phys. Rev.* **147** 332
Loh E 1967 *Phys. Rev.* **154** 270
Loh E 1968 *Phys. Rev.* **175** 533

[3] Lira A, Dagdug L, Méndez A, Murrieta H and Caldiño U G 1999 *Phys. Status Solidi* b **212** 199
[4] McKeever S W S, Jassemnejad B, Landreth J F and Brown M D 1986 *J. Appl. Phys.* **60** 1124
[5] Caldiño U G, Muñoz A F and Rubio J O 1990 *J. Phys.: Condens. Matter* **5** 6071
[6] McKeever S W S, Jassemnejad B, Brown M D, Mathur V K, Abbundi R J and Chan H 1986 *Radiat. Eff.* **99** 15
[7] McKeever S W S, Brown M D, Abbundi R J, Chan H and Mathur V K 1986 *J. Appl. Phys.* **60** 2505
[8] Dorenbos P and den Hartog H W 1985 *Phys. Rev.* B **31** 3939
[9] Alonso P J and Alcalá R 1981 *J. Lumin.* **22** 321
[10] Bril A, Klasns H A and Zalm P 1953 *Philips Res. Rep.* **8** 393
[11] Dexter D L 1953 *J. Chem. Phys.* **21** 836
[12] Blasse G 1969 *Philips Res. Rep.* **24** 131